Available online at www.sciencedirect.com
SCIENCE DIRECT
Sensors and Actuators B 113 (2006) 545–554
SENSORS AND ACTUATORS B CHEMICAL
www.elsevier.com/locate/snb

Low-cost microelectrode array with integrated heater for extracellular recording of cardiomyocyte cultures using commercial flexible printed circuit technology

Laurent Giovangrandi, Kristin H. Gilchrist [1], R. Hollis Whittington, Gregory T.A. Kovacs *

Department of Electrical Engineering, CIS-202X, Stanford University, Stanford, CA 94305-4075, USA

Received 7 October 2004; received in revised form 22 February 2005; accepted 15 March 2005
Available online 22 April 2005

Abstract

This article reports the use of commercial, flexible printed circuit technology for the fabrication of low-cost microelectrode arrays (MEAs) for recording extracellular electrical signals from cardiomyocyte cultures. A 36-electrode array has been designed and manufactured using standard, two-layer, polyimide-based flexible circuit technology, with electrode diameters of 75 and 100 μm. Copper structures defined on the backside of the array have been used for low-power thermal regulation of the culture. Electrical characterization of the gold-plated electrodes showed impedances below 250 kΩ at 1 kHz. Functional testing was conducted using HL-1 cardiac myocytes. The arrays proved biocompatible, and supported the formation of functional syncytia, as demonstrated by electrical recordings of depolarization waves across the array. A comparison with conventional, glass-based MEAs is presented, which reveals differences in signal strength (smaller for larger electrode) and variability (less for larger electrodes), but no effect of the substrate types on culture parameters such as beat rate or conduction velocity. The performance of the on-chip heating was evaluated, with typical temperature settling times (to ±0.1 °C) below 10 s, for a power consumption around 1 W (at 37 °C). Accuracy and stability are discussed. HL-1 cell responses to various temperature profiles enabled by the on-chip heating are presented, showing a remarkable correlation between temperature and beat rate.

Keywords: Microelectrode array; Flexible printed-circuit board; Temperature control; Cardiac myocytes; HL-1

1. Introduction

The extracellular electrical recording of electrogenic cells cultured over microelectrode arrays (MEAs) is a technique used increasingly over the last decade. As a fundamental research tool, it has been shown to yield valuable information on neuronal network and cardiac tissue dynamics. Recent reviews by Stett et al. [1] and Kovacs [2] provide numerous references and further illustrate the applications of microelectrode arrays in cell-based biosensors, drug discovery, and safety pharmacology.

Production of these microelectrode arrays has typically relied on thin-film technologies derived from the microelectronic manufacturing industry [3–7]. These technologies enable high-resolution (electrodes smaller than 10 μm) and high-density arrays (typically 32–64 electrodes with spacing down to 100 μm). However, none of these technologies are truly standard, resulting in high processing costs. Scalability is another issue, as the cost of the chips increases markedly with size, as do packaging costs with array element number. This is of particular importance for multi-well designs incorporating several arrays. Lastly, the current paradigm is to reuse MEAs multiple times, driven mainly by the cost of commercially available MEAs. In addition to concerns about degradation of the array and of its performance and cross-contamination between experiments, such recycling involves additional (and often underestimated) costs due to handling, cleaning, and inspection.

* Corresponding author. Tel.: +1 650 725 3637; fax: +1 650 725 5244.
E-mail address: kovacs@cis.stanford.edu (G. T.A. Kovacs).
[1] Present address: RIT International, 3040 Cornwallis Road, Research Triangle Park, NC 27709, USA.

0925-4005/$ – see front matter © 2005 Elsevier B.V. All rights reserved.
doi:10.1016/j.snb.2005.03.059

While some applications require the electrode size and density typically achieved by these conventional microelectronics technologies (e.g., detection of single neuron activity in neuronal cultures), others can accommodate larger electrodes with larger spacings. This is the case for cardiac myocyte cultures in particular, in which the electrode detects a traveling wave resulting from the depolarization of multiple, synchronized cells in a syncytium.

We have demonstrated a new generation of microelectrode arrays leveraging flexible printed-circuit board (flex-PCB) technologies. Flex technologies provide denser integration compared with their rigid counterparts, epoxy-based PCB technologies, with typical feature size of 3–4 mils (75–100 μm, high-end technologies enabling much smaller features are not considered here due to their associated higher cost). Flexible technologies primarily use polyimide (most common), polyester or liquid crystal polymer (LCP) as substrates, copper as conductors, photolithography, drilling and laser etching for patterning, and various metal finishes, including gold. In comparison to microelectronic manufacturing, these technologies have been optimized for larger circuits, lower resolution, and are highly standardized to achieve the low cost imposed by the high-volume markets. In that respect, they offer an excellent alternative for the fabrication of low-cost, single-use MEAs targeting cardiac applications, as this paper demonstrates. It should be noted that the approach presented is differentiated from the numerous prior examples of flexible multielectrode arrays involving flexible, polyimide films as substrates [8–10], which used custom, thin-film processes, and not commercial PCB technologies. An exception is the relevant work of Malkin and Pendley [11], who proposed a high-density microelectrode probe for in vivo cardiac mapping using the cross-section of a 20-layer flexible circuit board compatible with standard manufacturing.

The microelectrode array design integrates 36 gold-plated, circular microelectrodes 75 or 100 μm in diameter on a 50 μm-thick Kapton® substrate (polyimide). These dimensions, while not the smallest achievable with flex-PCB technology, represent a good price/performance ratio. In addition, the multilayer feature of the PCB technology has been used to integrate a heater and temperature sensor (based on the thermal coefficient of resistance of copper) using thin copper traces on the backside of the array, hence enabling temperature control of the active area. Integration of on-chip thermal heating and sensing has already been demonstrated in [7] using CMOS technology, and has shown exceptional stability and low power requirements. While this approach also enables integration of complex signal pre-processing and thermal management, it leads to expensive MEAs with the same issue of scalability discussed earlier. The proposed design enables on-chip heating at a minimal added cost.

The manufactured MEAs have been characterized both electrically and functionally. Electrical characterization included electrode impedance measurements, temperature sensor variability across MEAs and stability over time. Functional tests have been conducted with HL-1 cardiomyocyte cultures. The HL-1 cell line, derived from mouse atrial myocytes [12], has been extensively characterized on standard, glass microelectrode arrays in our lab with regard to both biochemical [13] and environmental sensitivity [14]. Using these previously collected data, a discussion of the performance of flex MEAs compared to standard MEAs bearing smaller electrodes of 10 and 22 μm is also given.

2. Methods

2.1. Flexible microelectrode arrays (Flex-MEAs)

The array layout was designed with the PCB design software Protel (Altium, Frenchs Forest, Australia). The generated Gerber files were then sent to PFC Flexible Circuits Limited (Scarborough, Ont., Canada) for fabrication in a standard two-layer polyimide technology. Fabrication time was 3 weeks (lead time for such a technology can typically be reduced to a few days, if requested). Specifications of the technology are given below. For clarity, dimensions related to the PCB are given in the industry standard, English units, doubled with metric units when necessary (note: 1 mil ≈ 25 μm). The substrate is an adhesiveless, 2 mil Kapton® film (Pyralux® series, DuPont™, Wilmington, DE) with 0.5 oz/ft^2 (equivalent to a thickness of 18 μm) copper layers on each side. The 1 mil thick coverlays (Pyralux® series) are comprised of 0.5 mil of an acrylic adhesive and 0.5 mil of Kapton®. Openings of 3 and 4 mils are laser-etched. Larger openings are drilled. The exposed copper is coated with 100–150 microinches (2.5–3.8 μm) of electroless nickel and 3–8 microinches (75–200 nm) of gold (Type III, grade A, >99.9% purity).

Minimal line width and spacing imposed by the selected technology are 3 and 4 mils, respectively, enabling an inter-electrode spacing of 380 μm. Thirty-six electrodes of either 3 mils (75 μm) or 4 mils (100 μm) were defined, covering a total area of 2 mm × 2 mm. In addition, two large reference electrodes were defined on opposite sides of the electrode array.

A heater and a temperature sense resistor were defined on the backside of the circuit by two interlaced copper traces using a minimum line width of 3 mils. The dense folding (air gap of 4 mils) enabled a trace length of 28 cm within a circular area of 1 cm diameter under the electrode area. With a copper thickness of 18 μm, the traces had a theoretical resistance of about 3.5 Ω. A schematic of the layout and a cross-section schematic of the structure are given in Fig. 1.

Two batches of circuits, targeting electrodes with diameters of 100 μm (4 mils) and 75 μm (3 mils), respectively, were ordered. Upon receipt, the flex-MEAs were cleaned with isopropyl alcohol and mounted on a rigid FR4 template. Single-in-line connectors were soldered to enable the electrical connection to a previously developed amplifier board via a zero-insertion-force (ZIF) socket. Finally, a 35 mm diameter Petri dish (Nalge Nunc International, Rochester, NY,

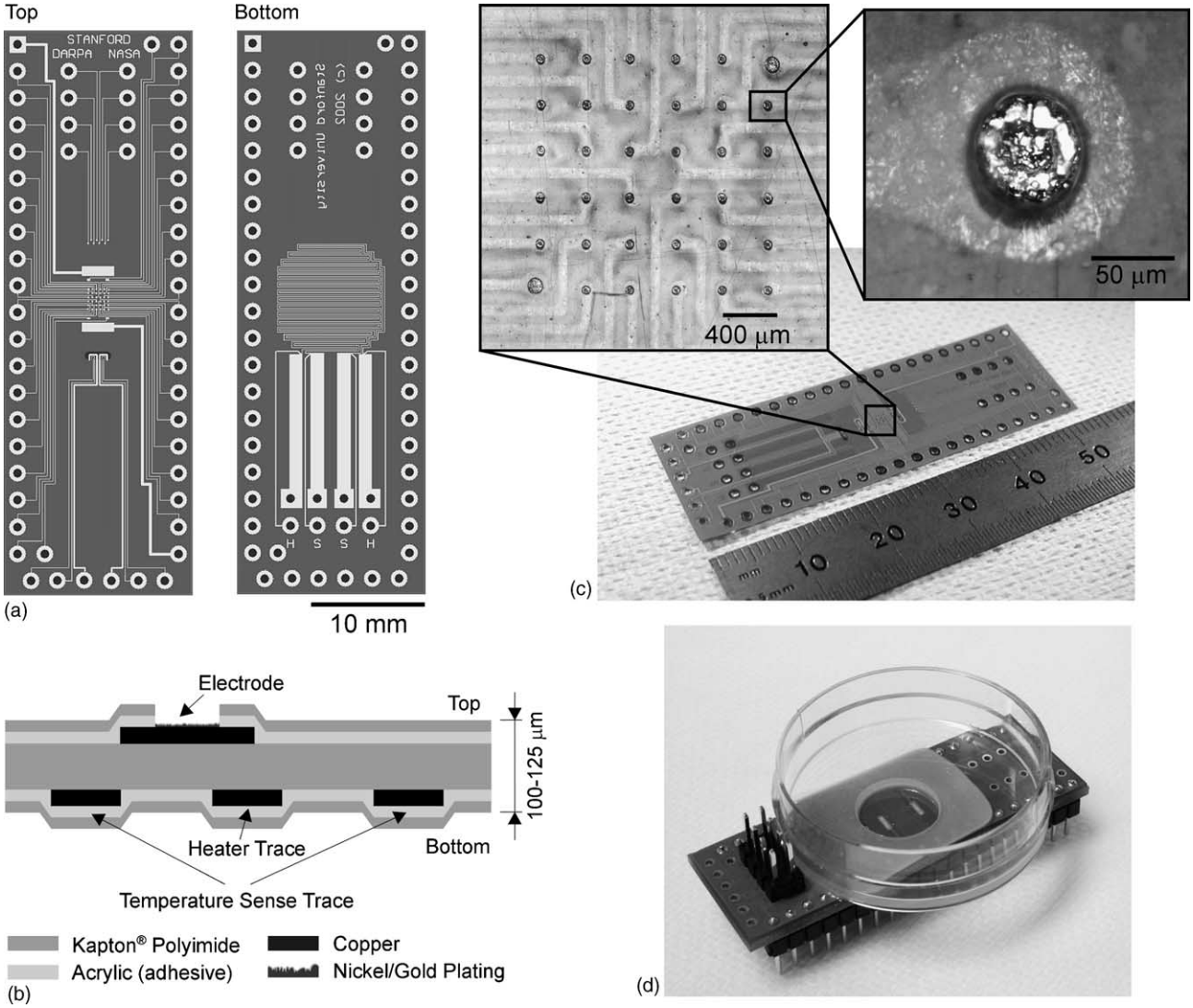

Fig. 1. Illustrations of the flex-MEAs: (a) CAD layout for top (electrode) and bottom (heater) layers; (b) cross-section schematics of the flex structure; (c) photograph of a flex-MEA as received from the manufacturer, with close-ups of the electrode area and of a 65 μm electrode; (d) photograph of an assembled flex-MEA, mounted on a rigid substrate with connecting pins and attached to a cell culture dish. The two large electrodes (635 μm × 2800 μm) visible in the center of the circuit are used to ground the culture bath during recording. The bottom pins connect the recording electrodes, while the top pins connect the heater and temperature sense traces.

USA) with a 10 mm diameter hole drilled in the bottom was glued (Supreme 42HT epoxy, Master Bond Inc., Hackensack, NJ, USA) on top to define the cell culture chamber. The final cartridge is shown in Fig. 1d. It should be noted that without the need to maintain compatibility with existing hardware, the design of the circuit can be greatly simplified to take advantage of card-edge connection systems, reducing the post-manufacturing assembly to simple gluing operations.

2.2. Impedance measurement

Measurement of electrode impedance was conducted on a custom impedance analyzer previously described in [15]. Briefly, a 50 mV_{p-p} AC voltage was used to drive the individual electrodes, and the resulting current (collected at the ground electrodes) was converted to a voltage, amplified, and separated into real and imaginary parts using a lock-in technique. The ground electrode's contribution to the measured impedance was negligible due to its large size compared to the individual electrodes (>500×). Known value resistors were used to calibrate the system. All measurements were conducted in phosphate buffered saline (PBS, 137 mM NaCl), after a 120 min hydration period.

2.3. Recording setup

Extracellular signals were amplified and filtered with a custom 36-channel amplifier, which has been described in detail in [16]. The amplifier had a gain of 1000×, and a band-pass characteristic with corner frequencies of 4 Hz and 3 kHz

for high- and low-pass, respectively. The amplified signals were digitized at 10 kHz. A thermal enclosure kept the MEA at a constant temperature (within 0.1 °C) when the on-chip heating capabilities were not used.

2.4. Temperature control circuit

The flex-MEA temperature was controlled using a custom circuit. Temperature measurement of the substrate was achieved with a four-point measurement of the temperature sense trace. Sensitivity after amplification was 6.4 mV/°C, assuming a thermal coefficient of resistance (TCR) for copper of 0.4%. Temperature control was performed using a proportional-integral (PI) error-circuit driving the heating trace. The system was interfaced to a computer, enabling logging and programmatic modulation of the temperature (steps, ramps, etc.), based on calibrated TCR and resistance at 25 °C (see Section 2.5). Noise reduction in the temperature measurements was achieved using a moving average filter (500 ms).

2.5. Temperature sense trace calibration

Calibration of the integrated temperature sense traces was performed using a 6.5-digit multimeter (A34401A, Agilent, Palo Alto, CA, USA) configured for four-wire measurement, and an external, calibrated temperature probe (type 554, YSI Inc., Yellow Springs, OH, USA) as reference. Measurement of resistance and temperature were simultaneously performed at steady-state after complete temperature stabilization (10–15 min). For full calibration (resistance at 25 °C and TCR), measurements were conducted at multiple temperatures, ranging from around 4 °C (in a refrigerator) to 40 °C, using a small regulated thermal enclosure (see [14]). For single-point calibration, the resistance at room temperature was measured, and the nominal resistance, referred to 25 °C, was calculated using an average TCR of 0.403%/°C.

2.6. Cell culture and experimental protocols

The HL-1 cell line, derived from mouse atrial myocytes [12], was used in all described experiments. Prior to seeding the cells, the microelectrode arrays were sterilized with 70% ethanol and coated with an adhesion-promoting solution containing 0.001% fibronectin (Sigma, St. Louis, MO, USA) and 0.02% gelatin (BD Biosciences, Sparks, MD, USA) and stored in a 37 °C incubator overnight. A suspension of HL-1 cells in culture media was obtained from a confluent flask of cells as described in [12]. The culture medium consists of Claycomb media (JRH Biosciences, Lenexa, KS, USA), supplemented with 10% fetal bovine serum (JRH Biosciences), 100 μM norepinephrine (Sigma), 100 units/ml penicillin-streptomycin (Invitrogen Corp., Carlsbad, CA, USA), and 4 mM L-glutamine (Invitrogen). The gelatin/fibronectin solution was aspirated from the arrays and replaced with the cell suspension. The cells were plated at a density of approximately 1200 cells/mm^2. The cultures typically reached confluence and showed spontaneous electrical activity two days after plating. Electrical recordings were performed between days 2 and 10 after plating.

For the evaluation of the stability of the temperature control and the resulting cellular response, a flow-through system and buffered medium were used to minimize osmolarity and pH variation. The flow-through setup consisted of a syringe pump (74900 Series, Cole Parmer Instrument Co., Vernon Hills, IL, USA) pushing media at a rate of 100 μl/min into the cell chamber, and a peristaltic pump (P720, Instech Laboratories Inc., Plymouth Meeting, PA, USA) evacuating the media out of the chamber. This configuration allowed for smoother flow compared to a peristaltic-only pumping. The media was buffered with 20 mM HEPES (Sigma, St. Louis, MO, USA), adjusted to pH 7.4 with NaOH.

Though flex-MEAs were typically designed for single use only, multiple uses have been performed for longevity studies. Following use, the arrays were cleaned for 60 min in a 5% detergent solution (Contrad® 70, Decon Laboratories Inc., Bryn Mawr, PA, USA), rinsed thoroughly in deionized water, sprayed with ethanol, blown dry with nitrogen gas and baked at 65 °C for 2 h for complete moisture removal.

2.7. Comparison with glass microelectrode arrays (glass-MEAs)

Recordings made on flex-MEAs were compared with previous recordings performed on microlithographically defined, glass-based microelectrode arrays (glass-MEAs). These arrays are more representative of conventional MEAs, with smaller and denser electrodes (10 and 22 μm diameter spaced by 100 μm), and more planar surfaces (2 μm silicon nitride passivation). Electrode impedance was in the 100 kΩ range (at 1 kHz) due to electroplating of platinum black. For more information regarding these arrays, the reader is referred to [17].

Comparisons were based on multiple signal parameters extracted from baseline activity. The extraction was performed using custom software operating in the Matlab® environment. Six parameters were selected for comparison: amplitude, amplitude ratio, duration, signal-to-noise ratio (SNR), beat rate, and conduction velocity. Amplitude was defined as the peak-to-peak voltage of each extracellular action potential (AP). Amplitude ratio was defined as the ratio of the amplitude of the two major strokes of the extracellular AP (upstroke to downstroke, as shown in Fig. 5b). The duration was defined as the width of the AP downstroke at 50% of its maximum amplitude. The SNR was defined as the ratio of the peak-to-peak amplitude of the AP to the peak-to-peak noise level (six times the standard deviation of the baseline). The local activation time (LAT) reference for each action potential was defined as the point of maximum negative slope of the extracellular AP. The beat rate was then defined as the inverse of the delay between two consecutive LATs. Finally, the conduction velocity was derived us-

ing a triangulation method based on the method described in [18].

Ten-second recordings from independent arrays/cultures were randomly selected for each group (10 recordings/group). Electrodes with SNR below 10, as well as occasional outliers detected by visual inspection, were rejected from the parameter extraction step. For each recording, the extracted parameters were averaged over time (10 s) and over the available electrodes. Resulting parameters were compared using a one-way ANOVA test (confidence level of 98%), with a multiple comparison test based on Tukey's honestly significant difference criterion.

3. Results and discussion

3.1. Structural and electrical properties of electrodes

Flex-MEAs were received in two batches. The first batch (100 μm target openings) had electrodes with a measured average diameter of 101.3 ± 4.3 μm (mean ± S.D., $n = 24$). The second batch (75 μm target openings), reportedly underetched, had electrodes with a measured average diameter of 65.2 ± 1.8 μm ($n = 25$). For accuracy, these electrodes are referred to hereafter as 65 μm electrodes. All electrodes were found to be recessed 15–20 μm below the surface, due to the thickness of the coverlay. Photographs of the arrays, electrode area and integrated package are shown in Fig. 1.

The electrode impedance displayed an expected behavior for metal electrodes in saline/physiologic solution [19], with a typical frequency dependence of $f^{-\alpha}$ ($\alpha = 0.95$) for the magnitude, and a phase roughly constant across the 0.5–5 kHz range (see Fig. 2). The magnitude at 1 kHz was 215.3 ± 70.3 kΩ (mean ± S.D., $n = 165$) for 65 μm diameter electrodes, and 154.7 ± 16.9 kΩ ($n = 165$) for the 100 μm diameter electrodes. The phase at 1 kHz was $-80.7 \pm 6.5°$ and $-82.1 \pm 3.5°$, for 65 and 100 μm diameter electrodes, respectively. The variation of electrode roughness associated with the plating process likely explains the spreading observed in the impedance magnitudes within batches. Nevertheless, it should be noted that these impedances are small enough to guarantee a low thermal noise level (under 2.5 μV_{RMS} over a 10 kHz range for the 65 μm electrodes), eliminating the need for impedance reduction techniques such as platinum black electroplating.

3.2. Temperature sense trace characterization

The temperature sense traces, used as resistive temperature detectors (RTDs), were characterized for resistance and thermal coefficient (TCR) variability, as well as for drift over time in culture conditions. Fig. 3 shows a typical calibration curve for one trace, from 4 to 40 °C. The linear fit has an R^2 value better than 0.9998, indicating very good linearity of the TCR. Measurements for multiple traces ($n = 8$, distributed between batches) gave a nominal resistance (at 25 °C) of 3.91 ± 0.21 Ω, and a TCR of 0.403 ± 0.007%/°C.

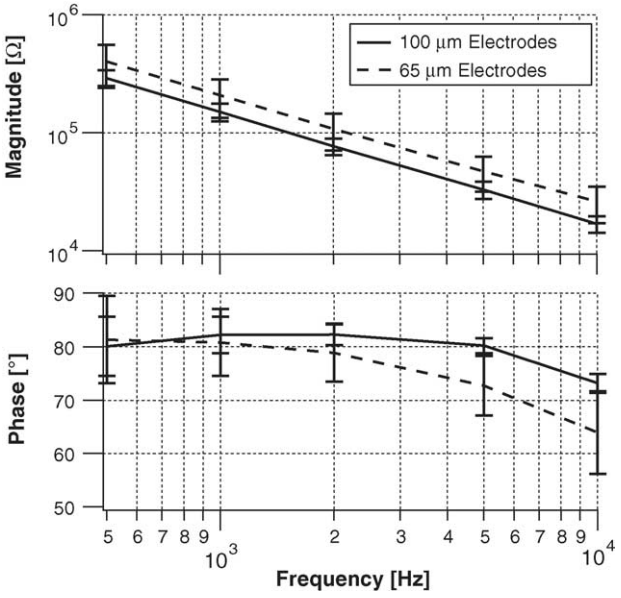

Fig. 2. Plots of the electrode impedance for the two sizes of electrodes (averaged spectra, $n = 165$ electrodes of each size). The frequency behavior is consistent with the behavior of a metallic electrode/electrolyte interface, with a decrease of the magnitude with frequency and a phase relatively constant around 1 kHz. Error bars are ± one sigma.

Drift under culture conditions has been characterized after 8 and 39 days. The substrates were stored immersed in PBS at 37 °C. A full calibration of the temperature sense traces was then performed as described in the Section 2. Results showed no significant drift of either the nominal resistance or the TCR over the tested period, as illustrated in Fig. 4.

The use of the copper layer of a standard PCB process for the integration of a heater, and in particular a temperature sensor, is subject to several conditions, including the stability of the thermal (TCR) and electrical properties (nominal resistance) over time, and to a lesser extent the reproducibility

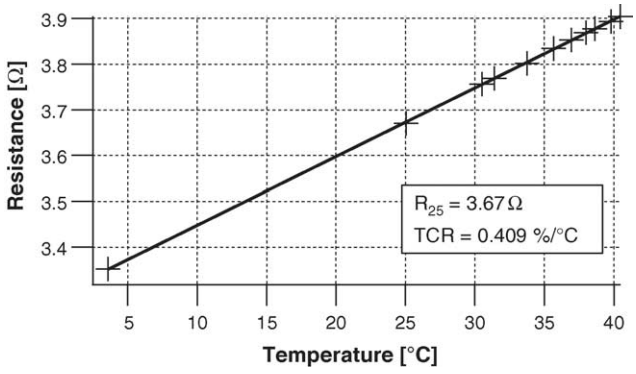

Fig. 3. Typical calibration curve of the resistance vs. temperature for a temperature sense trace (copper), measured between 4 and 40 °C. The R^2 value of the linear fit is 0.99998. Error bars are too small to be displayed. The average ($n = 8$) nominal resistance at 25 °C was 3.91 ± 0.21 Ω, and the average TCR was 0.403 ± 0.007%/°C.

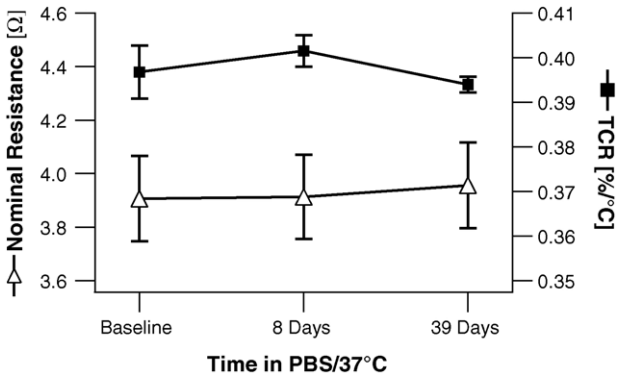

Fig. 4. Aging of the temperature sense traces under culture conditions (substrates stored in phosphate buffered saline at 37 °C). Plots of nominal resistance and TCR over time ($n = 4$). No significant change is noted. Error bars are ± one sigma.

of these properties between arrays. Stability over time is key to allow for a single initial calibration, used over the entire course of the experiment. Reproducibility across chips would remove the need for individual calibration. Results show that both the nominal resistance and the TCR are stable. However, the spread of the nominal resistance across chips (±5.4%) translates into an absolute error of ±1.26 °C at 37 °C (using a TCR of 0.403%/°C). On the other hand, the TCR shows a much better stability across chips (±1.7%), which translates into an absolute error of only ±0.21 °C at 37 °C (using a nominal resistance of 3.91 Ω).

A single-point calibration determining the nominal resistance, as used in this work, thus reduces the absolute temperature error to the single TCR error, which is less than ±0.25 °C over the useful range of 25–40 °C. The choice of the calibration method is ultimately dependent on the requirements of a specific application, but these results show that a single-point calibration of the integrated copper resistors leads to performance that should suit most cell-based applications.

3.3. Biocompatibility

Leveraging a standard technology for an application such as the one proposed here presents some major risks, most notably biocompatibility issues. This could arise from impure materials and contamination associated with the fabrication process, as well as from the properties of the materials in use. PCB fabrication is, for the large part, not done in a clean-room environment, and is thus more prone to external contamination. Also, the requirements on the material purity are less stringent than for clean-room processing. More specific to polyimide-based flexible circuits is the risk of potentially toxic copper ions [20] leaching out through the polyimide, known for its high water absorption (2 to 3% for standard polyimide as used here).

Of the 55 flex-MEAs tested to date, only two were found cytotoxic on their first use with HL-1 cells. This shows an apparent lack of systematic toxicity associated with the processing, as well as an inherent biocompatibility of the materials involved. It should be noted that the material biocompatibility is a result of careful pre-selection (data not shown) based on cell culture experiments with various types of PCB substrates. For instance, standard FR4/LPI (liquid photo imageable coverlay) showed inconsistent results from batch to batch, possibly due to more process-dependent surface (UV illumination and curing will influence the final chemical composition). Regarding long-term cytotoxicity, flex-MEAs were routinely used for three to four cell platings (runs) lasting between 7 and 9 days each. Except for the two devices found toxic at the first cell plating, all remaining devices supported cell growth for at least three runs (more than 21 days in culture), some extending up to six runs with successful electrical recording (38 days). The limiting factor appeared to be the catastrophic failure of the gold plating after three or more runs, with pieces of the gold plating lifting off from the large ground electrodes during the cleaning step. It should be noted that the cleaning itself might have contributed to the degradation of the circuits by mechanical (strong water rinse), or chemical (detergent with pH 12) means.

These results demonstrate the suitability of polyimide-based flex-MEAs to support HL-1 cell growth over the typical culture life cycle of 7 to 10 days. In addition, the arrays were found to be reusable to a certain extent, increasing their life span to several weeks if necessary. Longer uses might also be possible by improving the electrode plating (notably by using thicker gold platings), or modifying the cleaning protocol.

3.4. HL-1 signal recordings

Extracellular action potentials were successfully recorded from HL-1 cells plated on flex-MEAs with 100 μm electrodes (batch #1) and 65 μm electrodes (batch #2). Fig. 5 shows a recording of synchronous activity on 32 channels, with a local activation time (LAT) map showing continuous, uniform spreading of depolarization across the array. Average culture and AP parameters are given in Table 1 for the two sizes of flex-MEA electrodes. The recording of synchronous activity, and furthermore the observation of uniform spreading of the depolarization, shows that the fairly non-planar topography of the flex-MEAs (recessed electrodes) neither prevents the formation of a connected tissue, nor disrupts the signal propagation through the culture.

In terms of performance, Table 1 shows a comparison between flex-MEAs and glass-MEAs, bearing smaller, denser electrodes. First, the beat rate does not appear significantly different between size and type and does not exhibit any trend, showing the lack of influence of the microelectrode type on the beating properties of the HL-1 cultures. Similarly, no significant difference in the conduction velocity of the depolarization wave is noted. This is remarkable, as the interelectrode spacings and electrode sizes are vastly different, and it confirms again the development of a functional, connected syncytium on top of the flex-MEAs. The amplitude of the recorded signals shows an increase with smaller electrodes (though not significant), with an aver-

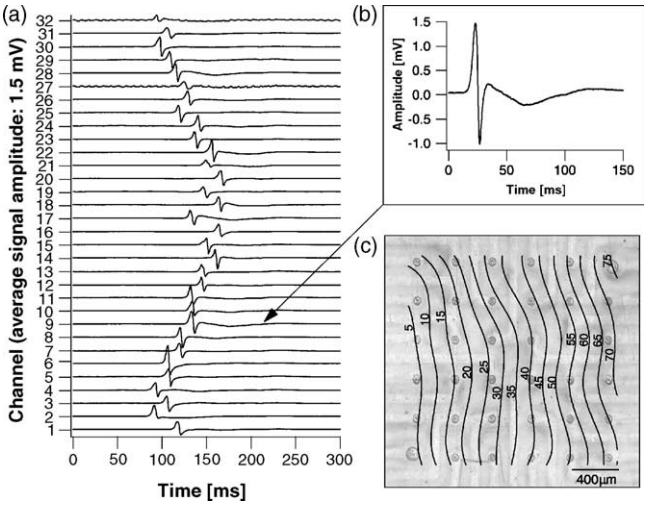

Fig. 5. Typical extracellular recording of HL-1 signals with a 100 μm electrode flex-MEA: (a) 32-channel snapshot of a depolarization wave; (b) close-up of an action potential showing the typical fast upstroke-downstroke followed by slower modulations; (c) isochronal map interpolated from the local activation time (LAT), showing a homogeneous propagation of the depolarization wave across the array (isochrone timings are given in milliseconds). The corresponding conduction velocity is 2.7 ± 0.4 cm/s (mean ± S.D., $n = 40$ triplets of electrodes). For reference, the picture of the electrode area is superimposed on the map.

age strength of 1.41 mV for 10 μm electrodes compared to 0.91 mV for 100 μm electrodes. However, action potential amplitude shows less variation on flex-MEAs, as seen by their lower standard deviation. As a consequence of the signal strengths, SNRs also appear smaller for flex-MEAs (still exceeding 15 on average), but more reproducible. Another interesting measurement is the upstroke/downstroke amplitude ratio, found to be significantly different between flex-MEAs and glass-MEAs. This reflects a systematic difference in the shape of the extracellular signal recorded, with signals more symmetrical on flex-MEAs on average, but also with more variability. With no obvious trend within the two MEA types, it is not clear whether this observation is a result of electrode size or electrode type. The duration of the downstroke appears not significantly different among the electrode sizes. Finally, it should be noted that the percentage of electrodes retained for analysis per MEA does not significantly differ between array types ($56 \pm 26\%$, $68 \pm 25\%$, $59 \pm 13\%$ and $66 \pm 21\%$ for 10, 22 μm glass-MEAs and 65, 100 μm flex-MEAs, respectively). Interestingly, some of these findings are consistent with the results of the work of Eason and Malkin [21], which shows simulated performances of various electrode size/spacing arrays. Indeed, they report a decrease of signal strength for larger electrodes and decreasing electrode size/spacing ratio (from 2.3 mV for 10 μm electrodes to 0.9 mV for 100 μm electrodes). This decrease, slightly higher than observed experimentally, is modeled by induced charges in an ideal electrode (with no electrochemical reaction), proportionally reducing the recorded signal (large electrodes have larger induced charge). Also, they show no significant impact of the electrode size/spacing on the measurement of the conduction velocity (although a slight, non-significant increase with electrode size, as measured in this study, is reported). However, the modeling of the maximum negative slope variation (larger values for smaller electrodes, at a constant electrode/spacing ratio) did not match our observations (data not shown), which showed no significant difference in slope.

This comparison shows that flex-MEAs are competitive with conventional MEAs for cardiac cell culture recordings. It also demonstrates that while there is motivation for small electrodes (signal strength, shape reproducibility), large electrodes (up to 100 μm) can provide similarly useful information at a lower cost.

3.5. Temperature control

Using the measured nominal resistance of the integrated temperature sense traces, the flex-MEAs were used together with the PI regulator to control the temperature of the substrate while simultaneously recording the electrical activity of the cells.

Fig. 6 shows two experiments emphasizing the fast settling times resulting from the small thermal mass of the system. The top graph shows a series of computer-controlled ramps (0.2 and 0.4 °C/s) and steps between 34 and 37 °C. The temperature measured by the temperature sense trace exhibits very rapid changes, with a settling time (to ±0.1 °C) of 5 s for the step and no overshoot. The temperature accuracy is better than 0.1 °C. The power required to keep the temperature of the substrate at 37 °C was only about one watt (ambient temperature of 25 °C). The cooling time for the 3 °C step down to 34 °C is under 10 s. Note that the dip in the temperature following the decreasing steps is caused by the integral term of the analog PI compensator. The cell response is illustrated by the beat rate and strictly follows the temperature,

Table 1
Summary of HL-1 culture and action potential parameters for the two electrode sizes of flex-MEAs, and the two electrode sizes of glass-MEAs

MEA type	Electrode diameter (μm)	Beat rate (Hz)	Conduction velocity (cm/s)	AP amplitude (mV)	AP stroke amplitude ratio	AP duration (ms)	SNR
Glass	10	3.40 ± 0.92	1.61 ± 0.4	1.41 ± 0.82	0.46 ± 0.10	5.90 ± 1.75	22.3 ± 11.7
	22	3.33 ± 0.64	1.83 ± 0.6	1.29 ± 0.88	0.50 ± 0.07	5.70 ± 1.45	22.4 ± 15.4
Flex	65	2.75 ± 0.49	1.91 ± 0.7	0.95 ± 0.52	0.72 ± 0.23	6.20 ± 1.75	17.0 ± 3.4
	100	3.07 ± 1.19	1.91 ± 0.5	0.91 ± 0.40	0.73 ± 0.24	6.02 ± 1.80	18.7 ± 3.2

See Section 2 for explanation of parameters and statistics. Mean and standard deviation are given for each parameter.

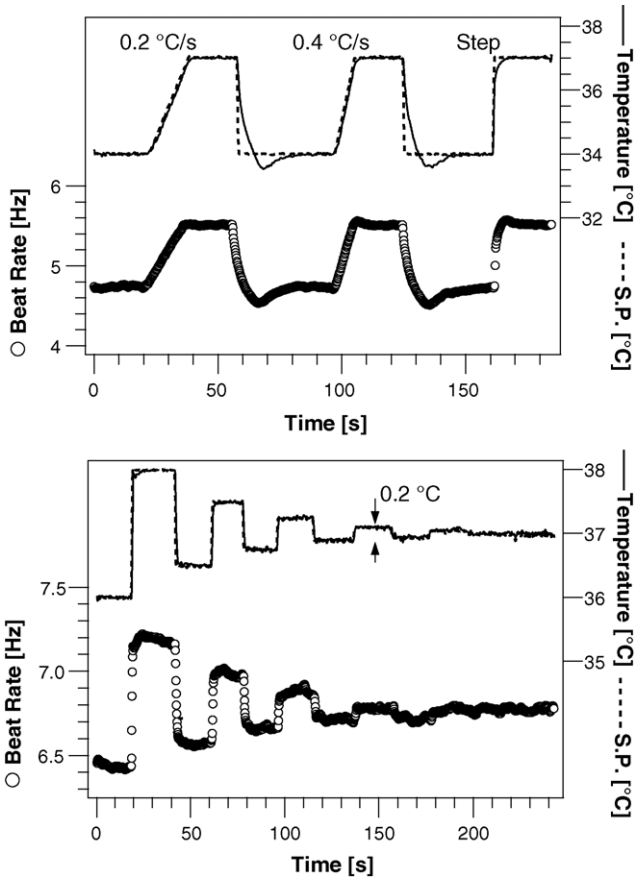

Fig. 6. Plots of the temperature step and ramp responses of HL-1 cells cultured on flex-MEAs with integrated heater. These experiments use the fast settling times resulting from the small thermal mass of the system to quickly change the temperature of the cell layer. The graphs show the temperature set point (S.P.), the actual temperature as measured by the temperature sense trace, and the beat rate of the HL-1 cells. Note how closely the beat rate follows the temperature profile: ramps generate linear increases; the step of 0.2 °C is still clearly visible in the beat rate; the correlation between the temperature steps and the beat rate steps in the bottom graph is better than 0.993.

alternating between 4.7 Hz at 34 °C and 5.5 Hz at 37 °C. A slight overshoot in the beat rate is visible following the step, and to a lesser extent following the 0.4 °C/s ramp. Similar results were obtained over five different cultures. The bottom graph further illustrates the high sensitivity of HL-1 cells to temperature, showing 20 s temperature steps with decreasing amplitude (2 °C down to 0.05 °C). The beat rate variation again strictly follows the temperature variation, with a correlation coefficient better than 0.993. The 0.2 °C step is clearly visible in the beat rate, while the 0.1 °C step is at the noise limit. Such sensitivity to temperature further exemplifies the need for a tight control of temperature in cell-based assays.

Experiments aimed at evaluating the stability of the temperature over time were also performed. Consistency is usually more important than accuracy with extracellular recordings, as most of the measurements are relative (referred to a baseline activity). Fig. 7 shows two experiments

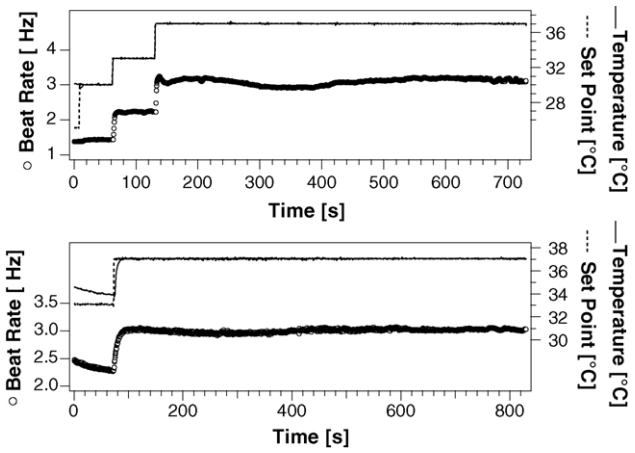

Fig. 7. Plots of the temperature control of HL-1 cells cultured on top of flex-MEAs using integrated heaters. The top graph shows the standard configuration of the flex-MEA. Some fluctuation of the beat rate (9.2%), related to surface temperature fluctuations, is visible. The bottom graph shows results for a flex-MEA with a heat diffuser on the back (see text for details). The step response is slower, but the stability of the beat rate (hence surface temperature) appears to increase (beat rate variation of 3.6%).

in which cells were rapidly brought to 37 °C and kept at that temperature for 10–12 min. The first experiment (top) uses the flex-MEA in the configuration described in the methods section. The temperature measured by the temperature sense trace exhibits very sharp steps, with settling times under 5 s, no overshoot, and an accuracy better than 0.1 °C at 37 °C. Following the 4 °C step from 33 to 37 °C, the beat rate of HL-1 cells increased by 0.88 Hz, which corresponds to a 10%/°C change. The beat rate response exhibits a small overshoot after the step to 37 °C, as seen previously in Fig. 6 (top), followed by slower perturbations, most likely reflecting fluctuations of the cell layer temperature itself. The variation in beat rate observed while at 37 °C is 0.28 Hz (9.2%). Using the 10%/°C factor previously calculated for the step to 37 °C as the conversion factor, this beat rate variation translates into a temperature variation of ±0.46 °C. These slow fluctuations, observed in all experiments ($n = 5$), were attributed to the thermal resistance between the heating and the sensing traces. To investigate this hypothesis, an experiment was carried out (Fig. 7, bottom graph) using a slightly modified configuration in which the heat transfer between the two traces was increased using a thin aluminum foil glued (using thermally conductive paste) on the bottom surface of the substrate. The resulting temperature profile is slightly slower (settling time of 20 s) as the thermal mass is increased, but the beat rate profile indeed appears more stable, with fluctuation at 37 °C of only 3.6%. Based again on the conversion factor derived from the step to 37 °C, this variation translates into ±0.19 °C, suggesting a positive effect of the heat diffuser. Of course, attributing the beat rate variation solely to temperature variation is to be considered a worst case here as the contribution of other biological fluctuations independent of temperature may be minimized but never totally cancelled. However, such an approach is imposed here due to the non-

trivial task of measuring accurately and non-invasively the temperature a few micrometers above the surface of the array in liquid.

In light of the lack of absolute measurements of the surface temperature, and because of the intrinsic variability in the cell response to temperature and other environmental variables (see [14] for a detailed analysis of these variations), we did not attempt to further quantify the performance of the system as measured by cellular response on a large scale in this study. However, while showing that some optimization might be required to get the best performance in terms of accuracy, these results clearly highlight the key features of the integrated heating, such as low power dissipation and fast settling times. Most importantly, these features come at a negligible cost, as opposed to previous work using specialized CMOS circuitry [7]. The spatial localization of the heating also enables multiple, independent arrays to be integrated on the same substrate in a multi-well configuration.

4. Conclusions

This work represents, to the best of our knowledge, the first demonstration of a planar microelectrode array for extracellular electrical recording based on an unmodified, commercial, flexible PCB technology. Manufactured MEAs showed consistent biocompatibility, supporting repeated HL-1 cardiomyocyte cultures for over 3 weeks. HL-1 signals were reliably recorded from these arrays and further demonstrated the formation of a functional syncytium, with beating and signal propagation characteristics similar to cultures observed on conventional, glass-based MEAs. The manufactured devices also incorporated on-chip heating capabilities demonstrating low-power, fast-response temperature control of the cell culture.

The use of a conventional, flexible circuit technology presents numerous advantages, including low cost (enabling single use), suitability for scaled-up designs (multi-array substrates), simplified packaging (monolithic device—no assembly except the culture chamber), straightforward compatibility with chip-on-board assembly (enabling on-chip processing using commercial integrated circuits such as multiplexers), and, as demonstrated in this work, integration of on-chip, low-power temperature control systems. In addition, utilizing a commercial channel allows easier access to MEA technology, as the only tool required is a PCB layout editor (freely available through the manufacturers); this approach also benefits from the PCB industry's fast turn-around times. The principal drawback is the relatively large electrodes and spacing compared with traditional MEAs, limiting their use to cardiac cultures, and potentially tissue slices. However, this technology is rapidly expanding its capabilities due to a constant push for denser integration of electronic components at low cost, and finer features will likely extend the application of this type of MEAs to neuronal cultures.

Acknowledgements

This work was supported by the DARPA Tissue-Based Biosensors program under contract no. N66001-99-C-8642, and by the NASA Ames Astrobionics program. The authors would like to thank William Claycomb and Proctor and Gamble for providing the HL-1 cells and protocols, Steve Kelly for his support with the PCB manufacturing process, John Hines for his general support on this project, and Janice Li, Nathalia Peixoto, Valerie Barker, and Tamara Doukas for contributing to this work.

References

[1] A. Stett, U. Egert, E. Guenther, F. Hofmann, T. Meyer, W. Nisch, H. Haemmerle, Biological application of microelectrode arrays in drug discovery and basic research, Anal. Bioanal. Chem. 377 (3) (2003) 486–495.
[2] G.T.A. Kovacs, Electronic sensors with living cellular components, Proc. IEEE 91 (6) (2003) 915–929.
[3] G.W. Gross, A.N. Williams, J.H. Lucas, Recording of spontaneous activity with photoetched microelectrode surfaces from mouse spinal neurons in culture, J. Neurosci. Meth. 5 (1–2) (1982) 13–22.
[4] W. Nisch, J. Böck, U. Egert, H. Hämmerle, A. Mohr, A thin film microelectrode array for monitoring extracellular neuronal activity in vitro, Biosens. Bioelectron. 9 (1994) 737–741.
[5] M.O. Heuschkel, Fabrication of Multi-Electrode Array Devices for Electrophysiological Monitoring of In-vitro Cell/Tissue Cultures, 13, Hartung-Gorre Verlag, Konstanz, Germany, 2001, p. 188.
[6] H. Oka, K. Shimono, R. Ogawa, H. Sugihara, M. Taketani, A new planar multielectrode array for extracellular recording: application to hippocampal acute slice, J. Neurosci. Meth. 93 (1) (1999) 61–67.
[7] B.D. DeBusschere, G.T.A. Kovacs, Portable cell-based biosensor system using integrated CMOS cell-cartridges, Biosens. Bioelectron. 16 (7/8) (2001) 543–556.
[8] R.S. Pickard, P.L. Joseph, A.J. Collins, R.C.J. Hicks, Flexible printed-circuit probe for electrophysiology, Med. Biol. Eng. Comp. 17 (2) (1979) 261–267.
[9] S.A. Boppart, B.C. Wheeler, C.S. Wallace, A flexible perforated microelectrode array for extended neural recording, IEEE Trans. Biomed. Eng. 39 (1) (1992) 37–42.
[10] M. Sandison, A.S. Curtis, C.D. Wilkinson, Effective extra-cellular recording from vertebrate neurons in culture using a new type of micro-electrode array, J. Neurosci. Meth. 114 (1) (2002) 63–71.
[11] R.A. Malkin, B.D. Pendley, Construction of a very high-density extracellular electrode array, Am. J. Physiol. Heart Circul. Physiol. 279 (1) (2000) H437–H442.
[12] W.C. Claycomb, N.A. Lanson Jr., B.S. Stallworth, D.B. Egeland, J.B. Delcarpio, A. Bahinski, N.J. Izzo Jr., HL-1 cells: a cardiac muscle cell line that contracts and retains phenotypic characteristics of the adult cardiomyocyte, in: Proceedings of the National Academy of Sciences of the United States of America 95 (6) (1998) 2979–2984.
[13] K.H. Gilchrist, L. Giovangrandi, G.T.A. Kovacs, Analysis of microelectrode-recorded signals from a cardiac cell line as a tool for pharmaceutical screening, in: Proceedings of the Transducers '01-Eurosensors XV, Munich, Germany, 2001.
[14] K.H. Gilchrist, L. Giovangrandi, R.H. Whittington, G.T.A. Kovacs, Sensitivity of cell-based biosensors to environmental variables, Biosens. Bioelectron. 20 (7) (2005) 1397–1406.
[15] D.A. Borkholder, N.I. Maluf, G.T.A. Kovacs, Impedance imaging for hybrid biosensor applications, in: Solid-State Sensor and Actuator Workshop, Hilton Head Island, SC, 1996.

[16] K.H. Gilchrist, V.N. Barker, L.E. Fletcher, B.D. DeBusshere, P. Ghanouni, L. Giovangrandi, G.T.A. Kovacs, General purpose, field-portable cell-based biosensor platform, Biosens. Bioelectron. 16 (7–8) (2001) 557–564.
[17] D.A. Borkholder, J. Bao, N.I. Maluf, E.R. Perl, G.T.A. Kovacs, Microelectrode arrays for stimulation of neural slice preparation, J. Neurosci. Meth. 77 (1997) 61–67.
[18] P.V. Bayly, B.H. KenKnight, J.M. Rogers, R.E. Hillsley, R.E. Ideker, W.M. Smith, Estimation of conduction velocity vector fields from epicardial mapping data, IEEE Trans. Biomed. Eng. 45 (5) (1998) 563–571.
[19] D.A. Robinson, The electrical properties of metal microelectrodes, Proc. IEEE 56 (6) (1968) 1065–1071.
[20] L.M. Gaetke, C.K. Chow, Copper toxicity, oxidative stress, and antioxidant nutrients, Toxicology 189 (1–2) (2003) 147–163.
[21] J.C. Eason, R.A. Malkin, A simulation study evaluating the performance of high-density electrode arrays on myocardial tissue, IEEE Trans. Biomed. Eng. 47 (7) (2000) 893–901.

Biographies

Laurent Giovangrandi received MS in microengineering and PhD in applied sciences from the Swiss Federal Institute of Technology (EPFL), Lausanne, Switzerland, in 1995 and 1999, respectively. His PhD thesis focused on microsystems for neuron-electronics interfaces and the control of cell-surface interactions. From 1999 to 2000, he worked as a research associate on planar patch clamp devices at the Institute of Physical Chemistry (ICP), EPFL. In 2000, he joined Stanford University to pursue a post-graduate research on cell-based biosensors and biosignal analysis. Since 2004, he has been working at the National Center for Space Biological Technologies (NCSBT), Stanford University, CA. His current interests include the application of cell-based microsystems in bioassays, drug screening and space research, as well as the analysis and visualization of biomedical signals.

Kristin H. Gilchrist received her BS in biomedical engineering from Vanderbilt University, Nashville, TN, in 1997, and MS and PhD in electrical engineering from Stanford University, Stanford, CA, in 1999 and 2003, respectively. Her PhD thesis research focused on cell-based biosensors utilizing cardiac cells cultured on microelectrode arrays. She is currently with the center for Materials and Electronic Technologies at RIT International in Research Triangle Park, NC. Her current research interests are in the development of novel microfabricated devices for chemical sensing and biomedical diagnostics.

R. Hollis Whittington received BS in electrical engineering from North Carolina State University, Raleigh, NC, in 1998, and MS in electrical engineering from Stanford University, Stanford, CA in 2002. He is currently pursuing PhD in electrical engineering at Stanford University. He joined MIT Lincoln Laboratory, Lexington, MA, in 1998 as a mixed-signal circuit designer for low-power charge-domain analog to digital converters. His current research interests at Stanford University include circuit and system design for biomedical instrumentation, cell-based biosensors, and drug-screening technologies, as well as electrophysiological instrumentation applied to cellular and tissue-level cardiology.

Gregory T.A. Kovacs received BASc in electrical engineering from the University of British Columbia, MS in bioengineering from the University of California, Berkeley, and PhD in electrical engineering and MD from Stanford University. He is a long-standing member of the Defense Sciences Research Council (DARPA), and has served as Associate Chair and Chairman. He also has extensive industry experience including co-founding several companies, including Cepheid in Sunnyvale, CA. He is a professor of Electrical Engineering at Stanford University with a courtesy appointment in the Department of Medicine His present research areas include biomedical instruments and sensors, miniaturized spaceflight hardware, and biotechnology. He is the Director of Medical Device Technologies for the Astrobionics Program at the NASA Ames Research Center, and Principal Investigator of the Stanford-NASA National Center for Space Biological Technologies. He helps direct a variety of projects spanning wearable physiologic monitors, biosensor instruments for detection of chemical and biological warfare agents and space biology applications, and free-flyer experiment payloads. In 2003, he served as the investigation scientist for the debris team of the Columbia Accident Investigation Board, having worked for the first 4 months after the accident at the Kennedy Space Center, Florida. In this role, he carried out physical, photographic, X-ray, chemical and other analyses on selected items from the nearly 90,000 pounds of recovered debris and worked toward understanding the nature of the accident. He currently serves as Engineering/Medical Liaison on the Spacecraft Crew Survival Integration Investigation Team (SCSIIT) of the Johnson Space Center. He received an NSF Young Investigator Award, held the Noyce Family Chair, and was a Terman and then University Fellow at Stanford. He currently is the Thomas V. Jones Development Scholar in the School of Engineering. He is a Fellow of the American Institute for Medical and Biological Engineering. He is a private pilot, scuba diver, and a Fellow National of the Explorers Club. He was a member of a NASA and National Geographic Society sponsored team that climbed Licancabur volcano (19,734 ft.) on the Chile/Bolivia border in November of 2003, serving as medical, physiologic research, and photography lead. In November of 2004, he served the same role on a return expedition to Licancabur, and carried out medical research and underwater videography in the summit lake.